








RESEARCH ARTICLE | JULY 13 2023

Machine learning opens a doorway for microrheology with optical tweezers in living systems

Matthew G. Smith ; Jack Radford ; Eky Febrianto; Jorge Ramírez ; Helen O'Mahony ; Andrew B. Matheson; Graham M. Gibson; Daniele Faccio ; Manlio Tassieri  



AIP Advances 13, 075315 (2023)

<https://doi.org/10.1063/5.0161014>

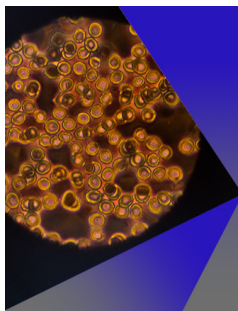


View
Online



Export
Citation

CrossMark



AIP Advances

Special Topic: Medical Applications
of Nanoscience and Nanotechnology

Submit Today!

Machine learning opens a doorway for microrheology with optical tweezers in living systems

Cite as: AIP Advances 13, 075315 (2023); doi: 10.1063/5.0161014

Submitted: 7 June 2023 • Accepted: 29 June 2023 •

Published Online: 13 July 2023



View Online



Export Citation



CrossMark

Matthew G. Smith,¹ Jack Radford,² Eky Febrianto,³ Jorge Ramírez,⁴ Helen O'Mahony,¹
Andrew B. Matheson,⁵ Graham M. Gibson,² Daniele Faccio,² and Manlio Tassieri^{1,a)}

AFFILIATIONS

¹ Division of Biomedical Engineering, James Watt School of Engineering, University of Glasgow, Glasgow G12 8LT, United Kingdom

² School of Physics and Astronomy, University of Glasgow, Glasgow G12 8QQ, United Kingdom

³ Glasgow Computational Engineering Centre, James Watt School of Engineering, University of Glasgow, Glasgow G12 8LT, United Kingdom

⁴ Departamento de Ingeniería Química Industrial y Medio Ambiente, Universidad Politécnica de Madrid, José Gutiérrez Abascal 2, 28006 Madrid, Spain

⁵ School of Engineering and Physical Sciences, Institute of Biological Chemistry, Biophysics and Bioengineering, Heriot Watt University, Edinburgh, United Kingdom

^{a)} Author to whom correspondence should be addressed: Manlio.Tassieri@glasgow.ac.uk

ABSTRACT

It has been argued that linear microrheology with optical tweezers (MOT) of living systems “*is not an option*” because of the wide gap between the observation time required to collect statistically valid data and the mutational times of the organisms under study. Here, we have explored modern machine learning (ML) methods to reduce the duration of MOT measurements from tens of minutes down to one second by focusing on the analysis of computer simulated experiments. For the first time in the literature, we explicate the relationship between the required duration of MOT measurements (T_m) and the fluid relative viscosity (η_r) to achieve an uncertainty as low as 1% by means of conventional analytical methods, i.e., $T_m \cong 17\eta_r^3$ minutes, thus revealing why conventional MOT measurements commonly underestimate the materials' viscoelastic properties, especially in the case of high viscous fluids or soft-solids. Finally, by means of real experimental data, we have developed and corroborated an ML algorithm to determine the viscosity of Newtonian fluids from trajectories of only one second in duration, yet capable of returning viscosity values carrying an error as low as $\sim 0.3\%$ at best, hence opening a doorway for MOT in living systems.

© 2023 Author(s). All article content, except where otherwise noted, is licensed under a Creative Commons Attribution (CC BY) license (<http://creativecommons.org/licenses/by/4.0/>). <https://doi.org/10.1063/5.0161014>

INTRODUCTION

Since their first appearance in the 1970s,^{1–3} Optical Tweezers (OTs) have been employed as extremely sensitive force transducers across a variety of disciplines within the *natural sciences*.^{4–9} OT rigs rely on the ability of a highly focused laser beam to optically trap in 3D micron sized dielectric particles suspended in a fluid. This is achieved by optically guiding a monochromatic laser

beam through a microscope objective with a high numerical aperture. Once trapped, the particle experiences a quadratic potential and therefore a restoring force that is linearly proportional to the distance of the particle from the trap center, with a constant of proportionality of the order of a few $\mu\text{N}/\text{m}$. Consequently, by measuring the particle position to a high spatial resolution (i.e., of a few nm), scientists have successfully measured forces as low as a few pN, such as those generated by the thermally driven motion of

water molecules¹⁰ or those exerted by single motor proteins.¹¹ Interestingly, accessing particles' trajectory to high temporal and spatial resolutions is one of the requirements underpinning microrheology techniques,^{12,13} as elucidated in this paper for the specific case of optical tweezers.

Microrheology is a branch of rheology (the study of the flow of matter) and is focused on the characterization of the mechanical properties of complex materials by performing measurements at micron length scales, often with sample volumes as little as a few microliters or even within living cells.¹⁴ This offers an indisputable advantage over classical bulk rheology techniques, which require milliliters of samples, especially in biophysical studies where samples are often rare and/or precious and come in small quantities (e.g., a few microliters). Microrheology techniques are categorized as either "passive" or "active" depending on whether the motion of the tracer particles is thermally driven or induced by an external force field, respectively. Interestingly, using optical tweezers is one such technique that can be defined as a *hybrid* microrheology tool¹⁵ because of the quadratic nature of the optical potential constraining the motion of the probe particle. Indeed, despite tracer particles being optically trapped (within the focal plane of a microscope), at short time scales (i.e., for small displacements), the restoring force exerted on the probe is weak enough for the particle to experience Brownian motion because of the thermal fluctuations of the molecules of the suspending media. Nonetheless, active microrheology with OTs is still possible either (i) by moving the trapping laser, often in a sinusoidal pattern, as elucidated in Refs. 16 and 17 or (ii) by using the transfer of spin angular momentum to govern the angular rotation of an optically trapped birefringent probe particle, as pioneered by Rubinsztein-Dunlop *et al.*^{18–20} However, as we shall further corroborate in this work, a necessary condition for executing either passive or active linear microrheology with optical tweezers (MOT) measurements is to perform "sufficiently" long measurements, commonly of the order of tens of minutes.^{17,21} This is because most of the analytical methods used to determine the materials' viscoelastic properties are underpinned by statistical mechanics principles, whose accuracy relies on the analysis of a *significant* number of independent readings. Therefore, as pointed out by Tassieri,¹⁷ it may not be appropriate to adopt MOT for studies involving living systems as biological processes occur at time-scales ranging from 10^{-2} to 10^2 s,^{22–25} and therefore, the viscoelastic properties of biological systems may not be considered time-invariant during the measurements. However, previous studies on microrheology of active actin-myosin gels²⁶ and of living cells²⁷ demonstrated that "for time scales less than 1 s," thermally excited motion dominates and the generalized Stokes–Einstein relation (that underpins passive microrheology methods) is still applicable. The above-mentioned statement was further corroborated in a recent publication by Hardiman *et al.*,²⁸ in which (i.e., Fig. 5) the normalized increment distributions evaluated at different lag-times are reported, which are near-Gaussian for short lag-times and broad tailed for longer lag-times.

Hence, the aim of this work is to explore modern Machine Learning (ML) methods to reduce the duration of MOT measurements and thus allow scientists to perform microrheology measurements in living systems. In order to achieve such a challenging aim, in this work, we have taken a first step toward a possible solution of the problem by focusing initially on the analysis of computer simu-

lated trajectories of an optically trapped particle suspended within a set of Newtonian fluids having viscosity values spanning three decimals, i.e., from 10^{-3} to 1 Pa s, before looking at some experimentally obtained trajectories. The goal was to develop a machine learning (ML) algorithm that would effectively estimate fluids' viscosity from relatively short measurements (≤ 1 s) and compare the outcomes with those obtained by analyzing the same set of data with conventional methods based on statistical mechanics principles.^{21,29–31} This study has led to the following key findings: (i) we corroborate the requirement for MOT studies to perform "sufficiently" long measurements when using conventional analytical methods for data analysis; (ii) we provide, for the first time in the literature, a means for estimating the required duration of the experiment to achieve an uncertainty as low as 1%; (iii) we provide evidence explaining why conventional MOT measurements commonly underestimate the materials' viscoelastic properties, especially in the case of high viscous fluids or soft-solids (e.g., gels and cells); (iv) we have developed an ML algorithm that uses feature extraction on only "one second" of trajectory data to determine the viscosity of Newtonian fluids, yet capable of returning viscosity values carrying an error as low as $\sim 0.3\%$ at best and of $\sim 7\%$ at worst, which is five times smaller than those obtained from conventional analytical methods applied to the same data.

THEORETICAL BACKGROUND

Passive microrheology with optical tweezers

Passive MOT is typically performed by means of a stationary optical trap that confines a spherical particle suspended in a fluid of unknown viscoelastic properties to 3D. At thermal equilibrium, the Brownian motion of the probe particle is caused by the thermal fluctuations of the fluids' molecules, and it is monitored by means of a high speed motion detection device. The particle trajectory is typically extracted in 2D, as the one shown in Figs. 1(b) and 1(c). A statistical mechanics analysis of the particle's trajectory can return not only the trap stiffness of the OT but also a good estimation of the frequency-dependent viscoelastic properties of the suspending fluid.^{21,29–35} The latter can be evaluated by solving a generalized Langevin equation as the following one:

$$m\ddot{\vec{a}}(t) = \ddot{\vec{f}}_{\vec{R}}(t) - \int_0^t \xi(t-\tau)\vec{v}(\tau)d\tau - \kappa\vec{r}(t), \quad (1)$$

where m is the mass of the particle, $\ddot{\vec{a}}(t)$ is its acceleration, $\vec{v}(t)$ is its velocity, $\vec{r}(t)$ is its position, $\ddot{\vec{f}}_{\vec{R}}(t)$ is the Gaussian white noise term used for modeling the stochastic thermal forces, and $\xi(t)$ is the generalized time-dependent memory function accounting for the viscoelastic nature of the fluid.³⁶ The convolution integral represents the time-dependent friction force exerted by the complex fluid onto the particle. The term $\kappa\vec{r}(t)$ is the restoring force of the optical trap when the confining field $E(\vec{r})$ exerted by the optical tweezers is assumed to have an harmonic form,

$$E(\vec{r}) = \frac{1}{2}\kappa\vec{r}^2, \quad (2)$$

where κ is the trap stiffness and \vec{r} is the particle position from the trap center. Interestingly, in the case of Newtonian fluids (i.e., for purely viscous fluids with constant viscosity η) and at low Reynolds

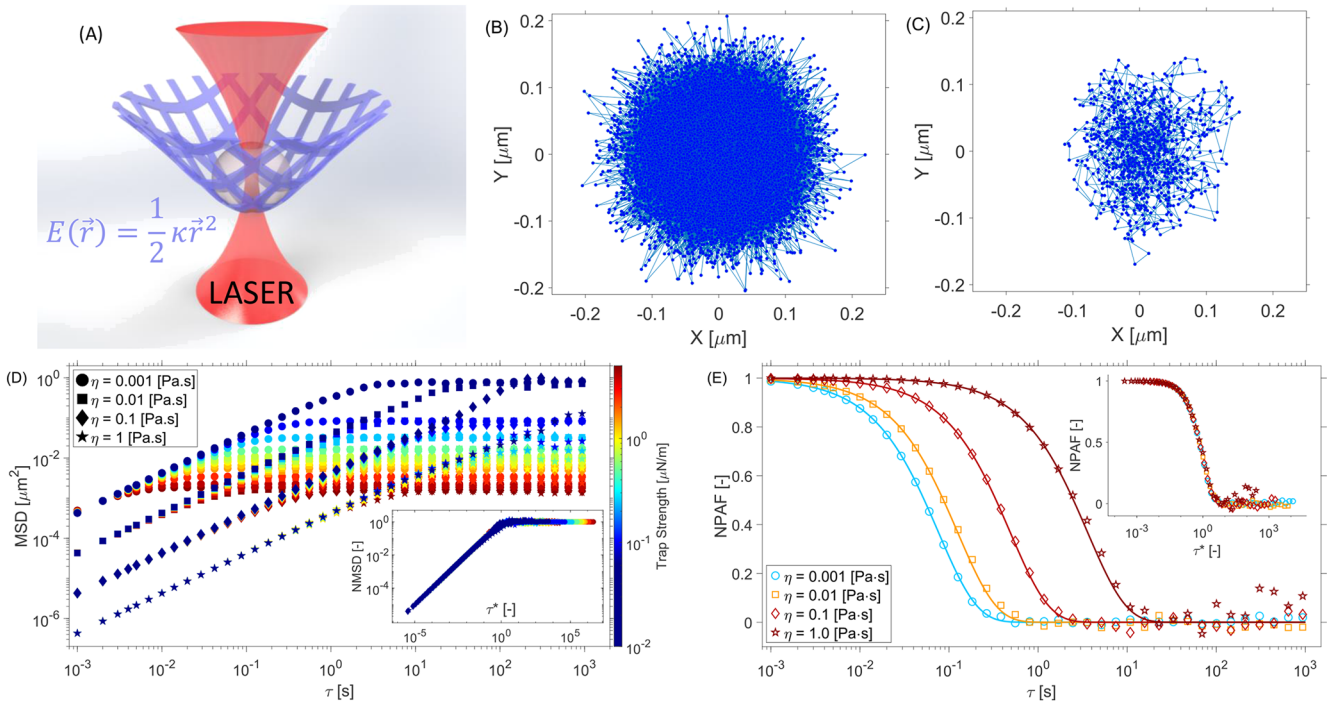


FIG. 1. (a) Schematic representation of an optically trapped bead within a harmonic potential, $E(\vec{r})$, where κ is the trap stiffness and \vec{r} is the bead position from the trap center. (b) and (c) Two examples of 2D trajectories of an optically trapped bead of a radius (R) of $1 \mu\text{m}$ suspended in water for 1024 s (b) and for 1 s (c). Both trajectories were generated by means of a MATLAB code adapted from the one developed by Volpe.³⁷ (d) The mean square displacement (MSD) curves of a series of 48 simulated trajectories of 1024 s duration and acquired at 1 kHz of an optically trapped particle experiencing constraining forces ranging from 0.01 to $5 \mu\text{N/m}$ (see the color bar) and suspended into four different Newtonian fluids having viscosity values spanning three orders of magnitude (see the legend). The inset shows the same data as in the main, but with the ordinate axis normalized by twice the variance of the particle trajectory and the abscissa τ replaced by the dimensionless lag-time τ^* , as elucidated in the body of the article. (e) Four examples of normalized position autocorrelation functions (NPAFs, symbols) of a particle suspended in four Newtonian fluids having viscosities of 10^{-3} , 10^{-2} , 0.1, and 1 Pa s and experiencing constraining forces of 0.25, 1.5, 4, and $5 \mu\text{N/m}$ [from left to right and color coded based on the color bar in (d)], respectively. The lines are single exponential decay functions $A(\tau) = e^{-\lambda\tau}$ drawn with $\lambda = \kappa / (6\pi\eta R)$ evaluated by using the input (nominal) parameters mentioned above; i.e., $\lambda = 13.26, 7.96, 2.12$, and 0.27 Hz, respectively. The inset shows the same data as in the main (symbols only), but the abscissa has been replaced by $\tau^* = \lambda\tau$.

numbers (for which the inertia term can be neglected), Eq. (1) is simplified as follows:³⁷

$$\vec{W}(t)\sqrt{2k_B T\gamma} = \gamma\vec{v}(t) + \kappa\vec{r}(t), \quad (3)$$

where the term on the left side represents the fluctuating force due to random impulses from many neighboring fluid molecules, $\gamma = 6\pi\eta R$ is the friction coefficient, R is the particle radius, k_B is Boltzmann's constant, and T is the absolute temperature. In this work, Eq. (3) has been adopted to generate (thousands of) 2D trajectories of optically trapped particles suspended into a set of Newtonian fluids having different viscosity values for machine learning purposes, as explained in the following sections.

In the general case, i.e., for any generic complex fluid, it has been shown^{29,30,32} that Eq. (1) can be solved for the fluids' complex shear modulus ($G^*(\omega)$) in terms of either the particle normalized squared displacement, $\Pi(\tau)$, or its normalized position autocorrelation function (NPAF), $A(\tau)$, which are both drawn in the insets of Figs. 1(d) and 1(e) for some of the cases studied in

this work. These two functions are simply related to each other, and their expressions are

$$\Pi(\tau) = \frac{\langle \Delta r^2(\tau) \rangle_{t_0}}{2\langle r^2 \rangle_{eq}} \equiv \frac{\langle [r(t_0 + \tau) - r(t_0)]^2 \rangle_{t_0}}{2\langle r^2 \rangle_{eq}} = 1 - A(\tau), \quad (4)$$

where τ is the lag-time ($t - t_0$) and the brackets $\langle \dots \rangle_{t_0}$ represent an average over all initial times t_0 . The relationship between the two above-mentioned time-averaged functions and the time-invariant fluids' complex shear modulus is

$$G^*(\omega) \frac{6\pi a}{\kappa} = \left(\frac{1}{i\omega\hat{\Pi}(\omega)} - 1 \right) \equiv \left(\frac{1}{i\omega\hat{A}(\omega)} - 1 \right)^{-1} \equiv \frac{\hat{A}(\omega)}{\hat{\Pi}(\omega)}, \quad (5)$$

where $\hat{\Pi}(\omega)$ and $\hat{A}(\omega)$ are the Fourier transforms of $\Pi(\tau)$ and $A(\tau)$, respectively. The inertial term ($m\omega^2$) presented in the original works^{29,32} has been neglected here because for micron-sized particles, it only becomes significant at frequencies of the order of MHz.

In the case of Newtonian fluids, the above-mentioned equations simplify significantly, and the relationship between the fluids' viscosity and the particle trajectory reads as follows:

$$\Pi(\tau) = 1 - A(\tau) = 1 - e^{-\lambda\tau}, \quad (6)$$

where $\lambda = \kappa/(6\pi\eta R)$ is the characteristic relaxation rate (also known as the "corner frequency"³⁸) of the compound system OT *plus* fluid. Moreover, it has been shown³¹ that by plotting $\Pi(\tau)$ and $A(\tau)$ vs a dimensionless lag-time $\tau^* = \tau\lambda$, all the curves having different values of η would collapse onto a master curve, as shown in the insets of Figs. 1(d) and 1(e), respectively. Consequently, for Newtonian fluids, it is a straightforward step to determine their viscosity by analyzing the temporal behavior of the NPAF.³¹ In particular, by plotting the natural logarithm of $A(\tau)$ vs τ , one would obtain a straight line having a slope equal to $-\lambda$, from which the viscosity could be determined by means of a simple linear fit. In this work, the fitting procedure has been constrained to ordinate values ranging from 0 and -1 (equivalent to $A(\tau) = 1$ and $A(\tau) = e^{-1}$) to minimize the error, as discussed hereafter.

METHODS

Simulation of particle trajectories

In order to train and test the machine learning algorithm discussed in the next section, we have used Eq. (3) to generate thousands of trajectories by means of a MATLAB code adapted from the one developed by Volpe,³⁷ which is able to simulate a 2D trajectory of an optically trapped particle suspended into a Newtonian fluid. The input parameters of the code were the trap stiffness, viscosity, temperature, particle radius, acquisition rate, and number of individual readings required. For instance, in Fig. 1, two examples of the trajectory having the same input parameters are shown, but the duration is 10^3 s in (b) and 1 s in (c).

Moreover, in order to investigate the impact of the measurement duration on the outcomes obtained from both the conventional and the ML enhanced MOT approaches, we generated a set of particle trajectories suspended into four different Newtonian fluids having viscosity values of 10^{-3} , 10^{-2} , 0.1, and 1 Pa s, respectively, and trap strengths ranging from 0.01 to $5 \mu\text{N/m}$. These trajectories were simulated for 1024 s at an acquisition rate of 1 kHz, which is equivalent to a real measurement of circa 17 min in duration. Due to their stochastic nature, it is possible to split each of these trajectories into shorter ones of variable duration, down to 0.05 s. All these trajectories were analyzed to calculate the fluids' viscosity by means of Eq. (6), and the mean absolute percentage error (MAPE) of the outcome was calculated for each trajectory by means of the following equation:

$$MAPE = \frac{100}{N} \sum_{i=1}^N \left| \frac{\eta_i - \eta_{0i}}{\eta_{0i}} \right|, \quad (7)$$

where N is the number of trajectories for a given duration, η_0 is the nominal viscosity value (used as input in the simulations), and η is the measured one.

Optical tweezer rig

Experimental measurements were performed by using an OT system based on a continuous wave, diode pumped solid state (DPSS) laser (Ventus, Laser Quantum), which provided up to 3 W at 1064 nm. A nematic liquid crystal spatial light modulator (SLM) (BNS, XY series 512×512) was used to create and arrange the desired optical trap. The laser entered a custom-made inverted microscope that uses a microscope objective lens (Nikon, 100 \times , 1.3 NA) to both focus the trapping beam and to image the thermal fluctuations of $4.74 \mu\text{m}$ diameter silica beads (Bangs Laboratories) at room temperature, $\sim 20^\circ\text{C}$. Samples were mounted on a motorized microscope stage (ASI, MS-2000). A complementary metal-oxide semiconductor (CMOS) camera (Dalsa, Genie HM 1024 GigE) acquired high-speed images of a reduced field-of-view. These images were processed in real-time at up to ~ 3 kHz to calculate the center of mass of the bead by using a particle tracking software developed in LabVIEW (National Instruments), running on a standard desktop PC.^{39,40}

Machine learning architecture

In fluid mechanics, machine learning (ML) has been widely used to translate observational and experimental data into knowledge about the underlying physics of fluids⁴¹ and their interactions with the environment.⁴² Depending on the information being used for learning, ML algorithms can be categorized into supervised, semisupervised, and unsupervised. In this work, we consider a supervised ML algorithm where the input (i.e., the particle trajectories) and the respective output (i.e., the viscosity) are used during learning. Specifically, we consider feed-forward neural networks (NNs), or multilayer perceptrons,^{43,44} as the nonlinear function approximation between the input and output. The standard feed-forward NNs pass the input information through a network of hidden units and activation functions to produce the prediction. Deep Neural Networks (Deep NNs)^{45,46} obtain a nonlinear approximation through the composition of multiple hidden layers. To obtain the unknown network weights, nonlinear optimization methods, such as backpropagation,⁴⁷ are used by minimizing the discrepancy between the predictions and the known training outputs.

In this paper, we sidestep the conventional method [i.e., Eq. (6)] of estimating fluids' viscosity from the trajectories of optically trapped particles by means of supervised ML. The training dataset consists of 100 000 particle trajectories, each of 10 s duration, for different fluid' viscosities. In order to cover the range of the explored viscosity (i.e., from 0.001 to 1 Pa-s), the viscosity values are randomly sampled from a log-uniform distribution ranging from 0.000 8 to 1.2 Pa-s. Similarly, the trap strengths are randomly sampled from a uniform distribution ranging from 0.08 to $0.39 \mu\text{N/m}$. Prior to the training, each trajectory coordinate input is normalized and flattened into a one-dimensional array. The normalization, i.e., subtracting the coordinates by their initial position, makes sure that there is no significant shift between the x - and y -component in the flattened array. Therefore, the flattening will have minimum effect on the trajectory's temporal correlation. Moreover, in this work, we also consider shorter observation times of the trajectories, i.e., $T_m = \{1, 0.5, 0.1, 0.05 \text{ s}\}$, which are obtained through subdivision of the original 10 s datasets.

Figure 2 shows a schematic representation of the ML architecture used in this study, consisting of two blocks, i.e., feature extraction and parameter estimation. The one-dimensional input, obtained by flattening the coordinates, is first processed through the feature extraction block, which comprises one-dimensional convolutional neural network (CNN) layers.^{48,49} These CNN layers serve as a convolution operator that enhances the local temporal structures present in the particle trajectories. In this study, two CNN layers are employed to eliminate the randomness of particle motion and highlight important features encoded in the trajectory. While it is possible to add more convolutional layers, we found that two layers are sufficient for the Newtonian fluid case. In each CNN layer, two filters with the same kernel width are used to increase the chances of identifying various features in the data. The filter widths are 10 and 100 for the first and second layers, respectively, which correspond to 0.01 and 0.1 s in the particle trajectory. The width increase in the second layer allows for filtering random motion with longer periods. Note that, for observation times $T_m = 0.1$ s and $T_m = 0.05$ s, the second convolutional layer filter sizes were adjusted, due to the shorter vector lengths, to 50 and 25, respectively. The resulting “feature maps” are transformations of the input data into latent variables, which highlight important information for the task of estimating the viscosity.

The feature maps are then concatenated, along with the trap stiffness and particle radius, to a 1D vector and passed to the parameter estimation block to predict the viscosity. The concatenation of additional variables is crucial to discriminate between fluids that have different viscosities but similar particle trajectories due to other dependent variables (e.g., trap stiffness and particle radius). Neural networks are known to be universal approximators,⁴³ and deeper layers often lead to a more expressive mapping or approximation. The number of layers and neurons is selected based on Occam’s razor principle⁵⁰ to ensure generalizability and prevent overfitting.

In this study, we identified that six fully connected dense layers provided a good estimate of the viscosity. Each neuron in the hidden layers uses a ReLu (rectified linear unit) activation function, while a linear activation function is used in the output layer. The loss function was chosen to be the mean absolute percentage error (MAPE) to prevent bias in training toward minimizing losses for high viscosity values with larger residuals. The hyper-parameters of the model including the batch size, learning rate, number of epochs, and validation split were 256, 10^{-5} , 200, and 0.1, respectively. Training has been performed in triplicate for each model with input trajectories having an interval T_m from 0.05 to 1 s, using an Adam optimizer,⁵¹ and was performed on a desktop PC equipped with an 18-core Intel i9-10980XE CPU (3 GHz), 256 GB RAM and an NVIDIA GeForce RTX 3090 with 24 GB memory. The training time for each ML model increased with decreasing input length due to the increasing number of training examples, so each model took from 2.5 to 6.5 h to train depending on the input trajectory.

RESULTS

One of the key features and advantages of using optical tweezers for microrheology purposes is that they can be easily calibrated without the use of external transducers. Indeed, as we shall discuss hereafter, it has been assumed^{21,29–34} that the trap stiffness of symmetric OTs can be determined to a high accuracy by appealing to the principle of equipartition of energy,

$$\frac{d}{2}k_B T = \frac{1}{2}\kappa\langle\bar{r}^2\rangle_{eq}, \quad (8)$$

where d is the dimension of the motion. This is true as long as the measurement time is “sufficiently” longer than the characteristic time τ_{OT} of the compound system made of an OT (i.e., its trap stiffness), fluid (i.e., its compliance), and beads (i.e., its radius taken

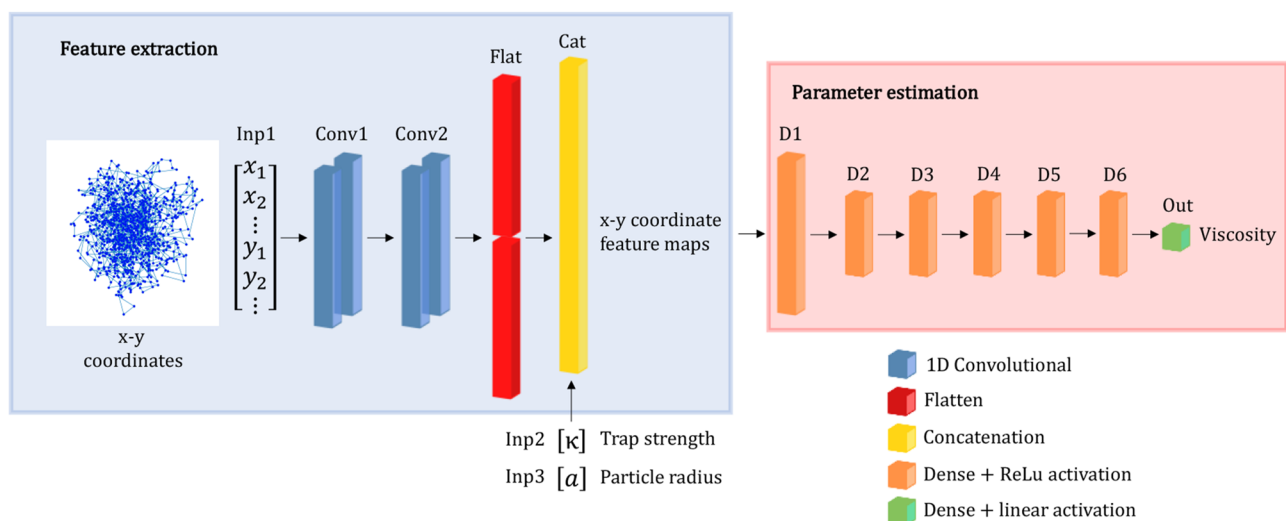


FIG. 2. Schematic representation of the machine learning architecture used in this work. A single particle trajectory of x - y coordinates is transformed and preprocessed for feature extraction, the output of which is concatenated with the trap strength (κ) and the particle radius (a). This is used as the input for parameter estimation with a single output node of viscosity.

as a characteristic length of the probe), which are not known *a priori* in rheological investigations of complex materials.

However, in the case of Newtonian fluids and operational condition of the instrument being within the micro length- and time-scales, as mentioned earlier, the compound system has a single characteristic time defined as $\tau_{OT} = \lambda^{-1}$, which can be used as a reference to estimate the minimum measurement duration required to properly calibrate the trap stiffness. In particular, by defining the duration of a measurement (T_m) as the ratio between the total number of readings (N) and the acquisition rate ($f = \text{samples/s}$) of the detector used for tracking the particle position, one could define the Deborah number⁵² for optical tweezers (De_{OT}) as

$$De_{OT} = \frac{\tau_{OT}}{T_m} = \frac{6\pi\eta Rf}{N\kappa}, \quad (9)$$

which can be further differentiated into “nominal” ($De_{OT,Nom.}$) and “effective” ($De_{OT,Eff.}$), depending on whether the trap stiffness used for determining λ is the nominal value set as the input in the simulation code generating the trajectories or the measured one by means of Eq. (8), which is affected by T_m , as demonstrated hereafter.

In Fig. 3(a) we report the ratio between the two Deborah numbers vs $De_{OT,Nom.}^{-1}$ for a series of 528 simulated trajectories of variable

duration of an optically trapped particle experiencing various constraining forces and suspended in four different Newtonian fluids having viscosity values spanning three orders of magnitude. Interestingly, the ordinate of such a diagram is equivalent to the ratio between the two trap stiffnesses $\kappa_{Nom.}/\kappa_{Eff.}$, while the abscissa is proportional to the measurement duration T_m . From Fig. 3(a), it is apparent that the existence of a crossover value of $De_{OT,Nom.} \sim 1$, delimiting two operating ranges of OT rigs, i.e., (i) for $De_{OT,Nom.}^{-1} \gg 1$, the trap stiffness is determined to a high accuracy via Eq. (8); (ii) for $De_{OT,Nom.}^{-1} \ll 1$, the constraining force is *undetermined*, or, more specifically, $\kappa_{Eff.}$ is *overestimated* as often happens in many real experiments for which T_m is not sufficiently long. Based on Eq. (5), consequently, when the trap stiffness is *overestimated*, the outcomes of MOT measurements are *underestimated*, especially when they are attempted in high viscous fluids or soft-solids (e.g., gels and cells).^{53,54} Our findings are further corroborated by the data shown in Fig. 3(b), where the absolute percentage error (APE) of $\kappa_{Eff.}$ is reported against $De_{OT,Nom.}^{-1}$ and compared with the experimental results (i.e., the horizontal line) reported by Matheson *et al.*,⁵⁵ representing the threshold value of the APE of $\kappa_{Eff.}$ below which microrheology measurements performed with OTs return an APE of the fluids’ viscosity lower than circa 5% (see Fig. 5 of Ref. 55). Consequently, based on a conservative approach, one could

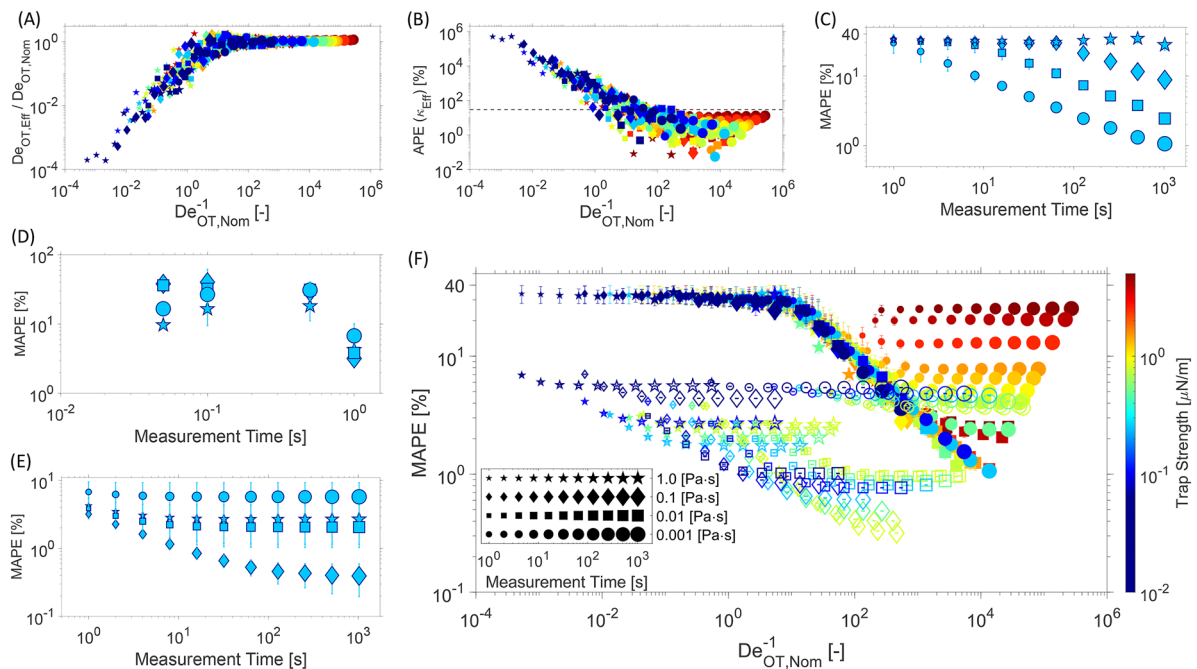


FIG. 3. (a) Ratio between the effective Deborah number for optical tweezers $De_{OT,Eff.}$ and the nominal one $De_{OT,Nom.}$ vs $De_{OT,Nom.}^{-1} \propto T_m$ for a series of 528 simulated trajectories of different durations of an optically trapped particle experiencing various constraining forces and suspended into four different Newtonian fluids having viscosity values spanning three orders of magnitude. (b) The absolute percentage error (APE) of $\kappa_{Eff.}$ vs $De_{OT,Nom.}^{-1}$ for the same set of trajectories as in (a). The line indicates an APE value of 30%, as reported in Ref. 55. (c)–(e) The mean absolute percentage error (MAPE) of viscosity vs measurement duration (T_m) determined (c) by using the conventional analytical method described in the body of the article, (d) by averaging the prediction error from ML algorithms with different input dimensions, and (e) by averaging the predictions of the three models with 1 s input dimension. [(f), closed symbols] The MAPE of viscosity vs $De_{OT,Nom.}^{-1}$ evaluated from the conventional approach applied to the same set of trajectories used in (a). [(f), open symbols] The MAPE of the optimal ML algorithm with an input measurement time of 1 s. The color bar indicates trap stiffness used during the generation of the trajectories. The size of the symbols scales with the measurement time as shown in the inset of (f).

argue that only for $De_{OT,eff} \leq 0.001$, an accurate calibration could be achieved, which implies a minimum measurement duration of $T_m \geq 1000 \times \tau_{OT}$ for a given system. For instance, in the case of two measurements, both performed at room temperature (i.e., $T = 20^\circ\text{C}$) with a bead of $1\ \mu\text{m}$ in radius and a trap stiffness of $\kappa = 2\ \mu\text{N/m}$, but one in water (with $\eta = 0.001\ \text{Pa s}$) and the other in a fluid having a viscosity thousand times higher than that of water (e.g., glycerol), the characteristic times of the two compound systems would be $\tau_{OT} \cong 0.01\ \text{s}$ and $\tau_{OT} \cong 10\ \text{s}$, respectively. Consequently, in order to achieve an accurate calibration of the OT (i.e., for $De_{OT} \leq 0.001$), the measurements should last at least $10\ \text{s}$ and $2.78\ \text{h}$, respectively.

At this point, it is important to highlight that optical tweezer rigs are commonly equipped with either a camera or a quadrant photodiode (QPD) device for tracking the particle position to a high acquisition rate, often operating at KHz or MHz, respectively. Consequently, when microrheology measurements are performed on materials with a higher viscous character than water, significantly longer measurements would be required, and therefore, rigs equipped with either a QPD or an ultra-high-speed camera would be more prone to be miscalibrated. This is because they are often equipped with an insufficient capacity of random access memory (RAM) to process the high-volume of data (of several MB/s) generated during the particle tracking procedure (of a possible duration of $T_m = 10^4\ \text{s}$, which would result in $>10\ \text{GB}$ RAM occupancy); thus, they either crash, or, in order to avoid this, measurements are stopped early, causing $De_{OT} \gg 1$. A possible solution to avoid memory clogging, but not the length of measurements, is achieved by equipping the rig with an online digital correlator, which allows the machine to process high-volume data streams and to compress the relevant information in real-time, thus minimizing the use of RAM.^{56,57}

Let us now investigate how T_m affects the evaluation of the fluid viscosity when it is determined using a conventional method. In particular, as introduced earlier, in the case of Newtonian fluids, it is a straightforward step to determine their viscosity by performing a linear fit of $\text{Ln}[A(\tau)]$ vs τ , which is executed for ordinate values ranging from 0 and -1 [equivalent to $A(\tau) = 1$ and $A(\tau) = e^{-1}$, respectively] to minimize the error. In Fig. 3(c), we report the mean absolute percentage error of the fluids' viscosity evaluated as mentioned above vs the measurement duration, which varies from 1 to 1024 s. The simulated trajectories were generated for optically trapped particles suspended into four fluids having viscosity spanning three orders of magnitude (i.e., from 0.001 to 1 Pa s), but all the other inputs have the following values: a trap stiffness of $0.25\ \mu\text{N/m}$, particle radius of $1\ \mu\text{m}$, constant temperature of 19°C , and acquisition rate of 1 kHz. From the diagram, it can be seen that for the short measurement duration (i.e., at $T_m = 1\ \text{s}$), all the measurements return an error as high as circa 33% whereas as the length of the measurement increases, the MAPE decreases to a remarkable value of only 1% at $T_m = 1024\ \text{s}$ for the fluid with the lowest viscosity value of 0.001 Pa s; however, for the other fluids, it would have required significantly longer measurements to reach a similar accuracy, as elucidated hereafter. Interestingly, when the same data shown in Fig. 3(c) are drawn against $De_{OT,Nom}^{-1} \propto T_m$, all the four curves collapse onto a master curve, as shown in Fig. 3(f) (closed symbols), together with the outcomes obtained from the same analysis as the

one described above, but applied to all the 528 simulated trajectories mentioned earlier, thus corroborating the concept introduced earlier that “the higher the fluid’s viscosity, the longer the measurement must be.” Moreover, from Fig. 3(f), it can be seen that at relatively low trap strengths, the MAPE of the viscosity decreases as T_m increases (i.e., for $De_{OT,Nom}^{-1} \gg 1$). However, at relatively high trap strengths, the error increases again, becoming almost independent of the duration of the measurement. This phenomenon can be explained in terms of the relative value assumed by the time-dependent fluid’s shear compliance ($J(t)$) to that of the “complex” system ($J_{cs}(t)$) composed by (i) the OT (whose contribution is purely elastic; i.e., κ), (ii) the viscoelastic fluid (whose contribution relies on its elastic and viscous components), and (iii) the particle radius a (which defines a characteristic length scale). In particular, when the suspending medium is a Newtonian fluid, $J(t)$ can be expressed as follows:^{30,58}

$$J(\tau) = \frac{\tau}{\eta} = \frac{\langle \Delta r^2(\tau) \rangle_{t_0} \pi R}{k_B T}, \quad (10)$$

where $\langle \Delta r^2(\tau) \rangle_{t_0}$ is the particle MSD, as introduced in Eq. (4). However, $J_{cs}(t)$ is proportional to $\Pi(\tau)$,³⁰ and it assumes the following analytical expression:

$$J_{cs}(\tau) = J_{OT} \left(1 - e^{-\lambda\tau}\right), \quad (11)$$

where $J_{OT} = 6\pi R/\kappa \propto \langle r^2 \rangle_{eq}$ is the time-independent compliance of the OT, which is inversely proportional to the trap stiffness and whose values are presented in Fig. 1(d) by the plateau values of the MSD curves. $J_{cs}(t)$ has been derived by combining Eqs. (6), (8), and (10), and it is presented by the $\Pi(\tau)$ data drawn in the inset of Fig. 1(d) for the same combination of fluids' viscosity and trap stiffness discussed above. From Eqs. (10) and (11), by dividing the second Maclaurin polynomial of $J_{cs}(t)$ by $J(\tau)$, one would obtain the following ratio:

$$\frac{J_{cs}(\tau)}{J(\tau)} = \left(1 - \frac{\tau}{\tau_{OT}}\right) \equiv \left(1 - \frac{J(\tau)}{J_{OT}}\right), \quad (12)$$

which provides a means for elucidating the high values of the viscosity MAPE at relatively high trap strengths, as reported in Fig. 3(c). Indeed, from Eq. (12), one could argue that at short lag-times, $J_{cs}(\tau) \cong J(\tau)$ if and only if $\tau_{OT} \gg \tau$ [or equivalently for $J_{OT} \gg J(\tau)$], which is true either for vanishing trap strengths [e.g., blue symbols in Fig. 1(d)] or for increasingly high viscous fluids [e.g., star symbols in Fig. 1(d)]. Therefore, given that the accuracy to which the viscosity is calculated depends on the number of data points of the NPAF [or equivalently of the MSD via Eq. (10)] available at lag-times $\tau < \tau_{OT}$ —i.e., within the time-window ranging from $\tau_1 = 1/f$ [for which $A(\tau_1) \sim 1$] to $\tau = \tau_{OT}$ [for which $A(\tau_{OT}) = e^{-1}$], used for the fitting procedure—the analysis of the particles' trajectory will return viscosity values with a high degree of uncertainty at relatively large κ values, for which $\tau_{OT} \rightarrow \tau_1$. Indeed, as shown in Fig. 1(d), for each fluid's viscosity, the effective time-window $[t_1, \tau_{OT}]$ shortens as the trap stiffness increases. From a physics perspective, this is simply because the stronger κ is, the smaller is the particle variance from the trap center [i.e., Eq. (8)], thus overshadowing the fluid's contribution to the particle dynamics. The above-mentioned concept

are in agreement with the Fickian approach adopted by Matheson *et al.*⁵⁹ to estimate the viscosity of Newtonian fluids via MOT measurements by determining the gradient of the MSD at the first two lag-times (i.e., $\tau_1 = 1/f$ and τ_2), for which they obtained an average error of $\sim 10\%$ [see Eq. (10) and related results in Fig. 5 of their article].

In order to better understand the *optimal modus operandi* of MOT measurements, it is thus important to analyze the relative position of the system's characteristic time within the "finite" experimental time-window. This concept was recently introduced by Tassieri *et al.*⁶⁰ while testing the efficacy of a novel analytical tool (i-Rheo GT) for converting the time-dependent materials' shear relaxation modulus into their frequency-dependent complex shear modulus. In particular, they introduced a dimensionless parameter $T_a = \log(\tau/t_1)/\log(t_N/t_1)$ that accounts for the relative position of the material's characteristic relaxation time τ to that of the experimental time window $[t_1, t_N]$, where t_1 is the shortest time of the experimental dataset (Here, $t_1 = 1/f$ and t_N is the longest one (here, $t_N \equiv T_m = N/f$)). The meaning of T_a is very similar in spirit to that of the renowned Deborah number (defined as the ratio between the material's characteristic time of relaxation and the time of observation), but it takes into account also the existence of a "finite" acquisition rate (i.e., of $f = 1/t_1$), and therefore, it can also assume negative values $\forall \tau < t_1$. Interestingly, in the context of this work, T_a assumes the following form:

$$T_a = \frac{\log(f\tau_{OT})}{\log(N)}, \quad (13)$$

and by plotting the MAPE of the viscosity vs T_a , as shown in Fig. 4, it is possible to identify a value of $T_a \approx 1/3$ where MAPE assumes a minimum. This could be used to express N as a function of De_{OT} via Eqs. (9) and (13), i.e., $N \approx De_{OT}^{-3/2}$, thus providing a means of estimating the number of data points to be acquired to achieve a MAPE of $\sim 1\%$ for any generic fluid. This is indeed possible if the trap stiffness of the OT rig is calibrated first in water and it is also assumed not to vary significantly when measurements are performed on different

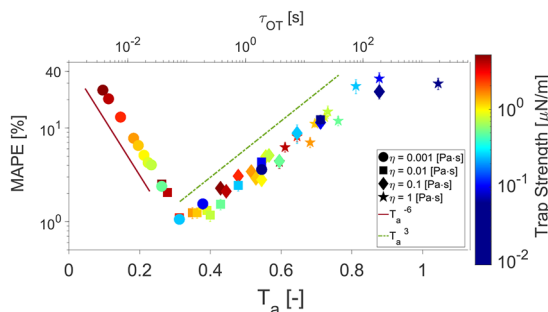


FIG. 4. Data taken from Fig. 3(f) for the trajectories with maximum T_m and drawn vs T_a . The top axis reports the characteristic time of the compound system τ_{OT} . The color bar indicates the nominal trap stiffness used during the generation of the trajectories. The two lines are guides for the power laws, as indicated in the legend.

fluids (i.e., when the refractive index of the sample under investigation does not differ significantly from that of water). With these conditions satisfied, one could write

$$N \approx N_w \eta_r^3, \quad (14)$$

where N_w is the number of positional data points acquired during the microrheology measurement performed in water (e.g., here $N_w \approx 10^6$) and $\eta_r = \eta/\eta_w$ is the relative viscosity of the fluid under investigation to that of water, of which an estimate is needed to determine N .

Moreover, from Fig. 4, it is interesting to notice that (i) for $T_a < 1/3$, the MAPE of the viscosity decreases with a power law of T_a^{-6} as $T_a \rightarrow 1/3$ from the left and that (ii) the data points adhering to this scaling law are mostly those obtained from trajectories drawn by using a low viscosity value as inputs (i.e., 0.001 Pa s) and relatively high trap stiffness as the outcomes diverge from the minima, thus implying that the MAPE of the viscosity in this region is governed mainly by the trap strength. However, for $T_a > 1/3$, the MAPE of the viscosity follows a power law of T_a^{-3} , and the data points adhering to this scaling law are mainly related to those trajectories drawn with a relatively low trap stiffness and relatively high viscosity, for which the measurement duration is not long enough for the bead to explore the whole potential well.

In summary, we can argue that microrheology with OT requires long measurement times with many individual readings to achieve the fluid's viscosity measurements with an error of only a few percent, which in practice translates to a measurement duration of the order of tens of minutes when dealing with fluids having viscosity close to that of water and OT rigs working at kHz and exerting a trap stiffness of the order of a few $\mu\text{N/m}$. When attempting microrheology measurements of fluids with significantly higher viscosity than water and under the same experimental conditions mentioned above, Eq. (14) reveals that the measurement duration would soon become "unachievable" because T_m scales with the cubic power of the relative viscosity: $T_m \approx T_{m,s} \eta_r^3$. These conclusions further corroborate Tassieri's "opinion"¹⁷ that conventional passive microrheology measurements with OT of living systems "are not an option" as biological processes occur at much shorter time scales than the required T_m , and therefore, their rheological properties could not be considered "time invariant" during the measurements. Thus, the aim of this paper is to employ machine learning algorithms to significantly shorten the duration of microrheology measurements performed with OT, as elucidated hereafter.

Enhanced MOT with machine learning

Let us now investigate the efficacy of ML algorithms when used to enhance the accuracy of viscosity measurement of Newtonian fluids in passive MOT measurements. It would be prudent here to highlight the change in language that will occur when discussing the aforementioned ML algorithms. Indeed, throughout the previous sections, the attainment of Newtonian viscosity by means of conventional analytical methods presented in Eqs. (1)–(4) has been justifiably described as "calculated." However, the ML algorithms described in this paper specifically "predict" the viscosity of the Newtonian fluid in question, and therefore, they will be described as such here.

As for the results described in Figs. 3(a), 3(c) and 3(f), the simulated trajectories used for evaluating the ML models were generated for optically trapped particles suspended into four fluids having viscosity spanning three orders of magnitude (i.e., from 0.001 to 1 Pa s). Figure 3(d) shows the MAPE of the fluids' viscosity prediction vs the measurement time, associated with input segment length, for the ML algorithms fed with the following inputs: the trap strength, particle radius, temperature, and acquisition rate have values of 0.25 $\mu\text{N/m}$, 1 μm , 19 $^\circ\text{C}$, and 1 kHz, respectively. It can be seen that for measurement times shorter than 1 s, using the architecture described in the Methods section, the MAPE is as high as 40% depending on fluid viscosity. Interestingly, for a measurement time of 0.05 s, the MAPE for the highest viscosity analyzed for $\eta = 1 \text{ Pa s}$ is 10%, which is four times lower than that of the conventional method using 1 s of trajectory. This is a striking result, considering that the characteristic time for that particular point, $\tau_{OT} \approx 75$, is around 1500 times larger than the measurement time. However, for $T_m = 1 \text{ s}$, the prediction error drops to between 3% and 6% across the three decades of fluid viscosity explored. Notice that the input measurement times used in this study did not exceed a value of 1 s because of the demanding computational processes involved in training ML algorithms. Therefore, in order to obtain consistent predictions of fluid viscosity, to extrapolate to 1024 s, the input measurement time used in Fig. 3(e) was 1 s. The extrapolation was carried out by feeding 1 s segments of particle trajectory into each of the three 1 s input ML models trained and averaging each of the predictions over increasingly longer times. The diagram shows the MAPE of the ML viscosity prediction vs the measurement time extrapolated to 1024 s using the same parameters described in Fig. 3(d). Generally, as the measurement time increases, the MAPE, starting at values between 3% and 6%, quickly drops to a plateau value for each viscosity, reaching as low as 0.4% for a viscosity of 0.1 Pa s. When compared to the conventional method shown in Fig. 3(c), the viscosity prediction errors displayed in Fig. 3(e) are significantly lower for most of the explored time windows, apart from the MAPE of the conventional approach at the longest times. It is important to highlight that in machine learning algorithms, the individual model accuracy is determined by the model hyper-parameters as well as the size and quality of training data. Moreover, the random initialization of the training process can cause the model to learn to predict particular viscosity ranges more accurately than others. The variability in performance of different instances of the same model for different viscosity values is indicated by the error bars in Figs. 3(d) and 3(e). The significant reduction in MAPE from the conventional approach to the ML prediction occurs over the entire range of explored viscosity.

As for standard ML studies, we have selected the best performing 1 s model to be analyzed for a range of trap strengths, as shown in Fig. 3(f). Here, the MAPE of both the conventional method (closed symbols) and the ML model (open symbols) is plotted vs $De_{OT,Nom}^{-1}$ for trap strengths ranging from 0.01 to 5 $\mu\text{N/m}$. Notice that the range of trap strengths used in ML analysis is 0.01–0.85 $\mu\text{N/m}$, which is slightly wider than the range of trap strengths used in training (0.08–0.39 $\mu\text{N/m}$). Figure 3(f) shows that the MAPE values of the ML algorithm are five times smaller than those of the conventional method for $De_{OT,Nom}^{-1} < 1$, i.e., $\sim 7\%$ and $\sim 35\%$, respectively. It is argued that ML enhances the accuracy of MOT because the learned mapping between measured features and predicted parameters can

be arbitrarily complex, and it is not restricted by approximations about the nature of the physical relationships. However, in the conventional case, there is a loss of information due to integration operations (e.g., averaging) and/or constraints (e.g., the linear best fit of the averaged data constituting the NPAF curve). Unlike the conventional method, the proposed ML-based approach is a fundamentally different inference method, which uses *prior* information gained from the training data to identify sensitive features in the raw measurements that are combined in a learned non-linear mapping to the targets; here, it is the fluid viscosity. From Fig. 3(f), it is also apparent that, unlike the conventional method, the ML error curves do not collapse into a master curve when drawn against $De_{OT,Nom}^{-1}$. This is believed to be due to the design of the feature extraction component of the ML architecture, which uses convolutional filters that learn local temporal structures common to both short and long trajectories. Therefore, once the model has learned to extract low- and high-dimensional local features in the measurements *a priori* during the training process, the CNN can decode the fluids' viscosity "directly" from the raw measurements using a statistically relevant number of steps N' required to disambiguate the features that are present in the data, rather than from statistically averaged quantities over $N = T_m f$ steps used in the standard approach. The number N' can be much smaller than N and no longer needs to satisfy the scaling governed by the Deborah number on the individual measurement as the missing information has been encoded before the measurement into the learned CNN parameters.

Confident about the effectiveness of the ML algorithm described above, we have employed it to determine the viscosity of water from real experimental MOT data obtained by tracking the position of an optically trapped bead subjected at different laser powers (i.e., trap strengths). The analysis of the trajectories returned the MSD curves shown in Fig. 5 having different plateau values at long lag-times, whose values are equal to twice the variance of the particle displacement from the trap center. These latter values can indeed be used to normalize the MSD curves, as shown in the top-left inset of Fig. 5, thus validating Eq. (11) stating that at long lag-times, the compliance of the OT overshadows the one of the fluid. In order to apply the ML algorithm to the raw data of the measurements described above, the simulated training data and the training of the model had to be adjusted to match the real experimental parameters, i.e., (i) an acquisition rate of 2780 fps, (ii) the length of the input data to 2780, to be consistent with the analysis of 1 s trajectory, (iii) the viscosity range has been narrowed to 10^{-3} – 10^{-2} Pa s, and their values were randomly sampled from a log-uniform distribution, and (iv) the values of the trap stiffness have been increased to a range of 1–5 $\mu\text{N/m}$, and they were randomly sampled from a uniform distribution. As for the simulated data described earlier, the ranges of viscosity and trap strength were slightly greater than the target range to encompass the extremities. When the ML algorithm was applied to real experimental data of 1 s duration, it returned an estimation of the fluid viscosity of $\eta_{ML} = 0.986 \pm 0.028 \text{ mPa s}$, which would result in an error as low as 1.1% at best, when compared with the viscosity value of water obtained by means of bulk rheology measurement, $\eta_{water} = 0.997 \text{ mPa s}$ (at $T = 20^\circ\text{C}$). The effectiveness of the method is further corroborated by the master curve drawn in the bottom-right inset of Fig. 5, where the NMSD curves have been plotted against a dimensionless lag-time $\tau_{ML}^* = \kappa\tau / (6\pi R\eta_{ML})$.

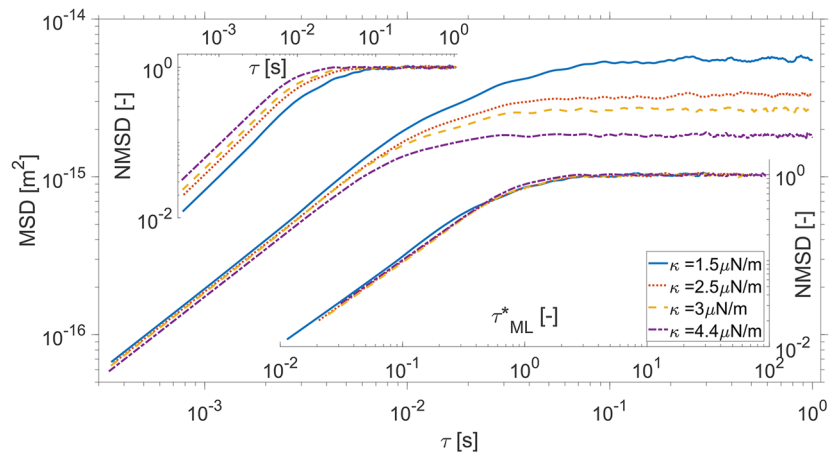


FIG. 5. (Main) Mean square displacement (MSD) vs lag-time τ of the trajectory of an optically trapped particle suspended in water and subjected to different trap strengths κ . (Top-left inset) The same data as in the main, but normalized by twice the variance of the particle displacement from the trap center, which returns the normalized mean square displacement (NMSD) vs τ . (Bottom-right inset) The same data as in the top-left inset, but vs a dimensionless lag-time $\tau_{ML}^* = \kappa\tau / (6\pi R\eta_{ML})$.

Therefore, we can argue that ML has the ability to enhance the accuracy of passive MOT measurements by significantly reducing the measurement time from tens of minutes down to 1 s with a prediction error that is five times smaller than the conventional analytical method applied to the same data. In addition, the ML algorithm shown here is able to predict the viscosity of a Newtonian fluid across the range of three decades, and we expect that a less generalized model, which is trained on a smaller span of viscosity values, could further improve the performance of the ML approach.

DISCUSSION

In this article, we provide experimental evidence supporting the observation made by Tassieri¹⁷ in 2015 that conventional linear microrheology with optical tweezers may not be an appropriate experimental methodology for studying the viscoelastic properties of living systems. In particular, we have focused on the analysis of computer simulated trajectories of an optically trapped particle suspended within a set of Newtonian fluids having viscosity values spanning three decimals, i.e., from 10^{-3} to 1 Pa s. The conventional statistical mechanics analysis of these simulations has led to the following key findings: (i) we corroborate the requirement for MOT studies to perform “sufficiently” long measurements when using conventional analytical methods for data analysis, (ii) we provide, for the first time in literature, a means for estimating the required duration of the experiment to achieve an uncertainty as low as 1%, and (iii) we provide evidence explaining why conventional MOT measurements commonly underestimate the materials’ viscoelastic properties, especially in the case of high viscous fluids or soft-solids such as gels and cells. Moreover, we have developed a machine learning algorithm that uses feature extraction on only “one second” of trajectory data to determine the viscosity of Newtonian fluids, yet capable of returning viscosity values carrying an error as low as $\sim 0.3\%$ at best, which is five times smaller than those obtained from conventional analytical methods applied to the same data. Our

results clearly indicate that machine learning is a valid option to be explored to perform fast and accurate microrheology measurements with optical tweezers in living systems.

ACKNOWLEDGMENTS

This work was supported by the EPSRC CDT in “Intelligent Sensing and Measurement” (EP/L016753/1). M.T. and A.B.M. acknowledge support via the EPSRC grant “Experiencing the micro-world - a cell’s perspective (Grant Nos. EP/R035067/1, EP/R035563/1, and EP/R035156/1).”

AUTHOR DECLARATIONS

Conflict of Interest

The authors have no conflicts to disclose.

Author Contributions

Matthew G. Smith: Conceptualization (equal); Data curation (lead); Formal analysis (lead); Investigation (lead); Methodology (lead); Software (lead); Validation (lead); Writing – original draft (lead); Writing – review & editing (equal). **Jack Radford:** Data curation (equal); Formal analysis (equal); Software (equal); Writing – original draft (equal); Writing – review & editing (equal). **Eky Febrianto:** Supervision (equal); Writing – original draft (equal); Writing – review & editing (equal). **Jorge Ramirez:** Methodology (equal); Writing – original draft (equal); Writing – review & editing (equal). **Helen O’Mahony:** Conceptualization (equal); Methodology (equal); Writing – original draft (equal). **Andrew B. Matheson:** Methodology (equal); Supervision (equal); Writing – original draft (equal); Writing – review & editing (equal). **Graham M. Gibson:** Methodology (equal); Supervision (equal); Writing – original draft (equal); Writing – review & editing (equal). **Daniele Faccio:**

Methodology (equal); Supervision (equal); Writing – original draft (equal); Writing – review & editing (equal). **Manlio Tassieri:** Conceptualization (lead); Data curation (equal); Writing – original draft (equal); Writing – review & editing (equal).

DATA AVAILABILITY

The data that support the findings of this study are available from the corresponding author upon reasonable request.

REFERENCES

- A. Ashkin, "Acceleration and trapping of particles by radiation pressure," *Phys. Rev. Lett.* **24**, 156–159 (1970).
- A. Ashkin and J. M. Dziedzic, "Optical levitation by radiation pressure," *Appl. Phys. Lett.* **19**(8), 283–285 (1971).
- A. Ashkin, J. M. Dziedzic, J. E. Bjorkholm, and S. Chu, "Observation of a single-beam gradient force optical trap for dielectric particles," *Opt. Lett.* **11**(5), 288–290 (1986).
- K. Svoboda and S. M. Block, "Biological applications of optical forces," *Annu. Rev. Biophys. Biomol. Struct.* **23**, 247–285 (1994).
- R. Diekmann, D. L. Wolfson, C. Spahn, M. Heilemann, M. Schüttel, and T. Huser, "Nanoscopy of bacterial cells immobilized by holographic optical tweezers," *Nat. Commun.* **7**(1), 13711 (2016).
- J. F. Davies and K. R. Wilson, "Raman spectroscopy of isotopic water diffusion in ultraviscous, glassy, and gel states in aerosol by use of optical tweezers," *Anal. Chem.* **88**(4), 2361–2366 (2016).
- Y. A. Ayala, B. Pontes, D. S. Ether, L. B. Pires, G. R. Araujo, S. Frases, L. F. Romão, M. Farina, V. Moura-Neto, N. B. Viana, and H. M. Nussenzweig, "Rheological properties of cells measured by optical tweezers," *BMC Biophys.* **9**(1), 5 (2016).
- W. J. Weigand, A. Messmore, J. Tu, A. Morales-Sanz, D. L. Blair, D. D. Deheyn, J. S. Urbach, and R. M. Robertson-Anderson, "Active microrheology determines scale-dependent material properties of chaetopterus mucus," *PLoS One* **12**(5), 1–19 (2017).
- H. Kim, W. Lee, H.-g. Lee, H. Jo, Y. Song, and J. Ahn, "In situ single-atom array synthesis using dynamic holographic optical tweezers," *Nat. Commun.* **7**(1), 13317 (2016).
- L. S. Madsen, M. Waleed, C. A. Casacio, A. Terrasson, A. B. Stilgoe, M. A. Taylor, and W. P. Bowen, "Ultrafast viscosity measurement with ballistic optical tweezers," *Nat. Photonics* **15**(5), 386–392 (2021).
- M. Capitanio, M. Canepari, M. Maffei, D. Beneventi, C. Monico, F. Vanzi, R. Bottinelli, and F. S. Pavone, "Ultrafast force-clamp spectroscopy of single molecules reveals load dependence of myosin working stroke," *Nat. Methods* **9**(10), 1013–1019 (2012).
- T. M. Squires and T. G. Mason, "Fluid mechanics of microrheology," *Annu. Rev. Fluid Mech.* **42**(1), 413–438 (2010).
- T. A. Waigh, "Microrheology of complex fluids," *Rep. Prog. Phys.* **68**(3), 685–742 (2005).
- B. D. Hoffman and J. C. Crocker, "Cell mechanics: Dissecting the physical responses of cells to force," *Annu. Rev. Biomed. Eng.* **11**(1), 259–288 (2009).
- M. Tassieri, *Microrheology with Optical Tweezers* (Jenny Stanford Publishing, 2016), pp. 235–272.
- M. T. Valentine, L. E. Dewalt, and H. D. Ou-Yang, "Forces on a colloidal particle in a polymer solution: A study using optical tweezers," *J. Phys.: Condens. Matter* **8**(47), 9477 (1996).
- M. Tassieri, "Linear microrheology with optical tweezers of living cells 'is not an option,'" *Soft Matter* **11**, 5792–5798 (2015).
- J. S. Bennett, L. J. Gibson, R. M. Kelly, E. Brousse, B. Baudisch, D. Preece, T. A. Nieminen, T. Nicholson, N. R. Heckenberg, and H. Rubinsztein-Dunlop, "Spatially-resolved rotational microrheology with an optically-trapped sphere," *Sci. Rep.* **3**(1), 1759 (2013).
- S. Zhang, L. J. Gibson, A. B. Stilgoe, I. A. Favre-Bulle, T. A. Nieminen, and H. Rubinsztein-Dunlop, "Ultrasensitive rotating photonic probes for complex biological systems," *Optica* **4**(9), 1103–1108 (2017).
- M. L. Watson, D. L. Brown, A. B. Stilgoe, J. L. Stow, and H. Rubinsztein-Dunlop, "Rotational optical tweezers for active microrheometry within living cells," *Optica* **9**(9), 1066–1072 (2022).
- M. Tassieri, "Microrheology with optical tweezers: Peaks and troughs," *Curr. Opin. Colloid Interface Sci.* **43**, 39–51 (2019).
- A. W. Harrison, D. A. Kenwright, T. A. Waigh, P. G. Woodman, and V. J. Allan, "Modes of correlated angular motion in live cells across three distinct time scales," *Phys. Biol.* **10**(3), 036002 (2013).
- D. Mizuno, C. Tardin, C. F. Schmidt, and F. C. MacKintosh, "Nonequilibrium mechanics of active cytoskeletal networks," *Science* **315**(5810), 370–373 (2007).
- T. Toyota, D. A. Head, C. F. Schmidt, and D. Mizuno, "Non-Gaussian athermal fluctuations in active gels," *Soft Matter* **7**, 3234–3239 (2011).
- B. Alberts, A. Johnson, J. Lewis, M. Raff, K. Roberts, and P. Walter, *Molecular Biology of the Cell*, 6th ed. (W.W. Norton and Company, 2015).
- D. Mizuno, D. A. Head, F. C. MacKintosh, and C. F. Schmidt, "Active and passive microrheology in equilibrium and nonequilibrium systems," *Macromolecules* **41**(19), 7194–7202 (2008).
- A. W. C. Lau, B. D. Hoffman, A. Davies, J. C. Crocker, and T. C. Lubensky, "Microrheology, stress fluctuations, and active behavior of living cells," *Phys. Rev. Lett.* **91**(19), 198101 (2003).
- W. Hardiman, M. Clark, C. Friel, A. Huett, F. Pérez-Cota, K. Setchfield, A. J. Wright, and M. Tassieri, "Living cells as a biological analog of optical tweezers—A non-invasive microrheology approach," *Acta Biomater.* **166**, 317 (2023).
- M. Tassieri, G. M. Gibson, R. M. L. Evans, A. M. Yao, R. Warren, M. J. Padgett, and J. M. Cooper, "Measuring storage and loss moduli using optical tweezers: Broadband microrheology," *Phys. Rev. E* **81**, 026308 (2010).
- M. Tassieri, R. M. L. Evans, R. L. Warren, N. J. Bailey, and J. M. Cooper, "Microrheology with optical tweezers: Data analysis," *New J. Phys.* **14**(11), 115032 (2012).
- M. Tassieri, F. D. Giudice, E. J. Robertson, N. Jain, B. Fries, R. Wilson, A. Glidle, F. Greco, P. A. Netti, P. L. Maffettone, T. Bicanic, and J. M. Cooper, "Microrheology with optical tweezers: Measuring the relative viscosity of solutions 'at a glance,'" *Sci. Rep.* **5**(1), 8831 (2015).
- D. Preece, R. Warren, R. M. L. Evans, G. M. Gibson, M. J. Padgett, J. M. Cooper, and M. Tassieri, "Optical tweezers: Wideband microrheology," *J. Opt.* **13**(4), 044022 (2011).
- A. Pommella, V. Preziosi, S. Caserta, J. M. Cooper, S. Guido, and M. Tassieri, "Using optical tweezers for the characterization of polyelectrolyte solutions with very low viscoelasticity," *Langmuir* **29**(29), 9224–9230 (2013).
- M. P. Lee, G. M. Gibson, D. Phillips, M. J. Padgett, and M. Tassieri, "Dynamic stereo microscopy for studying particle sedimentation," *Opt. Express* **22**(4), 4671–4677 (2014).
- M. G. Smith, G. M. Gibson, and M. Tassieri, "i-RheoFT: Fourier transforming sampled functions without artefacts," *Sci. Rep.* **11**(1), 24047 (2021).
- T. G. Mason and D. A. Weitz, "Optical measurements of frequency-dependent linear viscoelastic moduli of complex fluids," *Phys. Rev. Lett.* **74**, 1250–1253 (1995).
- G. Volpe and G. Volpe, "Simulation of a Brownian particle in an optical trap," *Am. J. Phys.* **81**(3), 224–230 (2013).
- K. Berg-Sørensen and H. Flyvbjerg, "Power spectrum analysis for optical tweezers," *Rev. Sci. Instrum.* **75**(3), 594–612 (2004).
- R. W. Bowman, G. M. Gibson, A. Linnenberger, D. B. Phillips, J. A. Grieve, D. M. Carberry, S. Serati, M. J. Miles, and M. J. Padgett, "'Red tweezers': Fast, customisable hologram generation for optical tweezers," *Comput. Phys. Commun.* **185**(1), 268–273 (2014).
- G. M. Gibson, J. Leach, S. Keen, A. J. Wright, and M. J. Padgett, "Measuring the accuracy of particle position and force in optical tweezers using high-speed video microscopy," *Opt. Express* **16**(19), 14561–14570 (2008).
- S. L. Brunton, B. R. Noack, and P. Koumoutsakos, "Machine learning for fluid mechanics," *Annu. Rev. Fluid Mech.* **52**(1), 477–508 (2020).
- L. J. Gibson, S. Zhang, A. B. Stilgoe, T. A. Nieminen, and H. Rubinsztein-Dunlop, "Machine learning wall effects of eccentric spheres for convenient computation," *Phys. Rev. E* **99**(4), 043304 (2019).

- ⁴³K. Hornik, M. Stinchcombe, and H. White, "Multilayer feedforward networks are universal approximators," *Neural Networks* **2**, 359–366 (1989).
- ⁴⁴C. M. Bishop and N. M. Nasrabadi, *Pattern Recognition and Machine Learning* (Springer, 2006), Vol. 4.
- ⁴⁵Y. LeCun, Y. Bengio, and G. Hinton, "Deep learning," *Nature* **521**(7553), 436–444 (2015).
- ⁴⁶I. Goodfellow, Y. Bengio, and A. Courville, *Deep Learning* (MIT Press, 2016), <http://www.deeplearningbook.org>.
- ⁴⁷D. E. Rumelhart, G. E. Hinton, and R. J. Williams, "Learning representations by back-propagating errors," *Nature* **323**(6088), 533–536 (1986).
- ⁴⁸Y. Lecun, B. Boser, J. S. Denker, D. Henderson, R. E. Howard, W. Hubbard, and L. D. Jackel, "Backpropagation applied to handwritten zip code recognition," *Neural Comput.* **1**(4), 541–551 (1989).
- ⁴⁹Y. Lecun and Y. Bengio, *Convolutional Networks for Images, Speech, and Time-Series* (MIT Press, 1995).
- ⁵⁰D. J. C. MacKay, *Information Theory, Inference and Learning Algorithms* (Cambridge University Press, 2003).
- ⁵¹D. P. Kingma and J. Ba, "Adam: A method for stochastic optimization," *arXiv:1412.6980* (2014).
- ⁵²M. Reiner, "The Deborah number," *Phys. Today* **17**(1), 62 (1964).
- ⁵³J. C. Ashworth, J. L. Thompson, J. R. James, C. E. Slater, S. Pijuan-Galitó, K. Lis-Slimak, R. J. Holley, K. A. Meade, A. Thompson, K. P. Arkill, M. Tassieri, A. J. Wright, G. Farnie, and C. L. R. Merry, "Peptide gels of fully-defined composition and mechanics for probing cell–cell and cell–matrix interactions in vitro," *Matrix Biol.* **85–86**, 15–33 (2020).
- ⁵⁴L. C. Geonzon, M. Kobayashi, M. Tassieri, R. G. Bacabac, Y. Adachi, and S. Matsukawa, "Microrheological properties and local structure of *t*-carrageenan gels probed by using optical tweezers," *Food Hydrocolloids* **137**, 108325 (2023).
- ⁵⁵A. B. Matheson, T. Mendonca, G. M. Gibson, P. A. Dalgarno, A. J. Wright, L. Paterson, and M. Tassieri, "Microrheology with an anisotropic optical trap," *Front. Phys.* **9**, 621512 (2021).
- ⁵⁶T. Yanagishima, D. Frenkel, J. Kotar, and E. Eiser, "Real-time monitoring of complex moduli from micro-rheology," *J. Phys.: Condens. Matter* **23**(19), 194118 (2011).
- ⁵⁷J. Ramirez, S. K. Sukumaran, B. Vorselaars, and A. E. Likhman, "Efficient on the fly calculation of time correlation functions in computer simulations," *J. Chem. Phys.* **133**(15), 154103 (2010).
- ⁵⁸J. Xu, V. Viasnoff, and D. Wirtz, "Compliance of actin filament networks measured by particle-tracking microrheology and diffusing wave spectroscopy," *Rheol. Acta* **37**(4), 387–398 (1998).
- ⁵⁹A. B. Matheson, T. Mendonca, M. Smith, B. Sutcliffe, L. Paterson, P. A. Dalgarno, A. J. Wright, and M. Tassieri, "An analytical framework for 3D microrheology measurements using an optical trap," *Research Square* (2022).
- ⁶⁰M. Tassieri, J. Ramirez, N. C. Karayiannis, S. K. Sukumaran, and Y. Masubuchi, "i-Rheo GT: Transforming from time to frequency domain without artifacts," *Macromolecules* **51**(14), 5055–5068 (2018).